33rd Annual International Conference of the IEEE EMBS
Boston, Massachusetts USA, August 30 - September 3, 2011

Time-Domain Ultra-Wideband Synthetic Imager (TUSI) in Silicon

Amin Arbabian and Ali M. Niknejad
Berkeley Wireless Research Center (BWRC), EECS Dept., UC Berkeley
Berkeley, CA

Abstract— **This paper introduces a silicon-based imaging array for remote measurements of complex permittivity of tissue. Using a coherent pulsed measurement approach, this time-frequency resolved technique recovers the three dimensional mapping of electrical properties of the subject in the microwave/millimeter-wave frequency spectrum. Some of the major challenges in the design of the system are described. Initial measurement results from the prototype high-resolution transmitter fabricated in a 0.13 μm SiGe process are described. The transmitter achieves pulse widths suitable for millimeter-level accuracy imaging.**

Index Terms— **Microwave medical imaging, silicon-based imaging device, dielectric measurements, millimeter-wave imaging, phased-array, beamforming, 90GHz reflection sensing, ultra-wideband.**

I. Introduction

As silicon transistors become faster, smaller and cheaper, many new medical applications for this technology emerge. In particular, operation at frequencies from 10 GHz - 200 GHz are possible in today's commercial technologies, and in the future this frequency limit will move closer to 500 GHz, entering the THz spectrum.

Although with great potential, electrical properties and polarization in the microwave/mm-wave frequencies have not received much attention for diagnostic imaging. There are specific applications where the information from electrical characteristics can greatly enhance image quality for detection and screening. As an example, electrical properties of malignant breast cancer and normal breast tissue are shown to be different [1] mainly due to the differences in vascularization levels. As another example, rotational modes of large protein structures show resonances in the microwave and millimeter-wave frequencies and this could be used for imaging and spectroscopy.

Microwave imaging of biological tissue for clinical [1], diagnostic and research applications has faced several major obstacles in terms of obtaining the required signal quality and resolution and this has severely limited progress and applications. Bulky devices and equipment have been utilized to obtain images using microwave frequencies. However, today's advances in the silicon industry, driven by economy of scale, allow for realization of low-cost arrays and processing units that can handle large computational problems. In addition to that, design of fully-integrated microwave and millimeter-wave systems have been made possible in scaled silicon processes [2] [3].

Here we describe the design of a time-based reflection sensing imager working in the microwave and millimeter-wave frequencies [4] [5]. The transmitter uses narrow pulses to sense the dielectric properties of the tissue. A first transmitter prototype has been implemented in a $0.13\mu m$ SiGe process and achieves pulse widths down to 26ps. This imager is totally self-sufficient and can be implemented at a fraction of the cost and size of alternate modalities. It is envisioned to be hand-held and completely portable and could address many scenarios where portability outweighs the benefit of higher resolution/quality or deeper signal penetration in tissue of other modalities. It could also provide specific benefits in cases where the contrast mechanism is superior to conventional means.

II. Dielectric Imaging in Microwave/mm-wave Spectrum

In any imaging modality, a specific property of the tissue is mapped to to the final image (e.g. tissue denisty/atomic number for X-ray or water content for MRI). One of the tissue properties that has not received the same level of attention is the macroscopic dielectric properties. These are the tissue response to relatively weak electromagnetic fields dominated by electric properties of ensemble of cells. Charge asymmetry and rotational mobilities cause electric dipole moments that respond to the external electric field differently based on the properties of tissue.

The main obstacle in measurement of dielectric properties has been the low penetration of microwave fields in human body. Higher frequencies that yield better (diffraction limited) resolution have even higher losses. The dynamic range for obtaining such images has not been attainable with standard measurement instruments. With the accelerated pace of growth in silicon and electronic devices, reaching the required dynamic range is becoming a possibility.

A. Contrast

Given the water content of human body, if used as a whole body imager, this technique will mainly deliver contrast based on water content. As a general-purpose imager, in terms of resolution and signal penetration, this technique will be inferior to MRI. However, dielectric contrast has been shown to provide great advantages in fatty tissue. For example, previous studies [1] have shown normal and malignant breast cancer tissue to have considerable contrast in the microwave frequency range. In addition, applications where the target is close to the skin could benefit from this technique.

978-1-4244-4122-8/11/$26.00 ©2011 IEEE

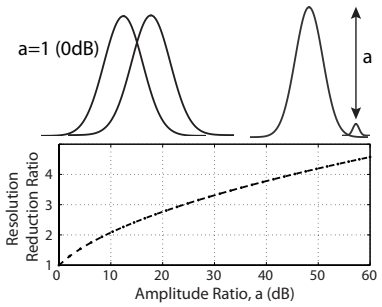

Fig. 1. Resolution reduction effect from large variations in amplitude. Here resolution the reduction ratio is shown normalized to the case of $a = 0dB$.

B. Low-Cost Breast Cancer Screening

Worldwide, breast cancer is the second most common type of cancer after lung cancer. Women in the United Stated have the highest incidence of breast cancer in the world and among them this is the most common cancer and the second most common cause of death [6] [7] .

Currently, mammography (X-ray imaging of compressed breast) is the dominant modality in early detection schemes. According to [7], some of the limitations of mammography are missing up to 15% of breast cancers, difficulty with women with dense breasts, and large false positives (as high as 10-15%). 10% of mammograms result in inconclusive data, only 10% of which turns out to be malignancies. The technique causes discomfort, is not widely available, and due to the ionizing radiation, poses health risks. Ionizing radiation limits the frequency of test to 18-24 months and is only performed for the specific age bracket of +40 years old. These are major obstacles in detecting fast-growing invasive cancers.

Using microwaves to detect cancerous tissue relies on the difference in dielectric properties of malignant and normal tissue. Since the dielectric properties could be different by a factor of 2-3[1], this allows for a reliable detection scheme. The antenna array uses UWB signals in several frequency bands to detect the tumor. The lower frequency bands are used to provide better penetration and are better suited for the cases that require depth of operation (10-15cm), while higher frequencies provide better resolution (mainly for areas closer to the skin).

C. Resolution

In the case of reflection measurements for medical applications, the resolution limit is tighter than the classical two-point radar resolution. This is due to the presence of a large reflection (from the skin) close to the potential target.

Resolution limits generally address two issues: ability to distinguish close objects (with same or different amplitudes) and the ability to pinpoint the position of an object in the presence of noise. It will be shown that both resolution limits improve with enhancing the signal bandwidth (BW).

Similar to radar analysis, it could be argued that the two point resolution of our imager for two equi-amplitude signals will be $\frac{c\tau}{2}$ (for pulsewidth of τ) or equivalently

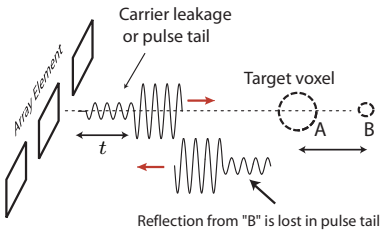

Fig. 2. Effect of pulse integrity on performance (echo effect shown here).

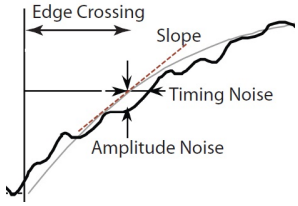

Fig. 3. Received pulsed edge with noise.

$\frac{c}{2BW}$ (where *BW* is the signal bandwidth) [8]. If the two signals have different amplitudes, especially in the case where one completely dominates the other, this becomes more restricting. Fig.1 shows the effect of obtaining lower resolution with larger amplitude ratios. For example, if a target is 40 dB lower than a main reflector, the resolution decreases by approximately a factor of 4. We therefore need to either push for narrower pulse generation (more BW) or compensate the effect with assumed prior knowledge of pulse shape. The former is difficult especially that this puts a limit on pulse fidelity and pulse amplitude roll-off in time domain (Fig.2). The latter requires better knowledge of dispersion characteristics. Without taking the effect of large amplitude ratios into account, to obtain resolutions close to 1mm in the human body the pulse width has to get close to 20ps. It is therefore necessary for this system to utilize calibration/compensation algorithms to achieve the resolution limit.

Resolution is also restricted from accurately identifying a pulse edge position. We can calculate the Cramer-Rao lower bound (CRLB) for the estimation of the pulse arrival time (and from that the position through $R_0 = vt_0/2$ where v is the wave propagation velocity). We will assume a white noise or equivalently colored noise with sampling at nulls of the auto-correlation function. The lower bound on the timing uncertainty can be derived as:

$$\overline{(t_0)^2} = \frac{1}{\beta^2 \frac{E}{N_0/2}} \tag{1}$$

Where *v* is the speed of wave propagation in the medium, *E* the pulse energy, N_0 the noise spectral density and β is an effective bandwidth [9]. Once again, a sharper and narrower pulse results in a better decision on the pulse arrival time. This result can be explained by Fig.3. An edge from a pulse of width τ and rise time t_r is shown together with additive noise. The quantity to be estimated is the arrival edge of the pulse. The amplitude noise gets "translated" to timing

uncertainty through the slope of the pulse edge and hence:

$$\overline{{t_0}^2} = \frac{\overline{n^2}}{slope^2} = \frac{\overline{n^2}}{A^2/t_r^2} = \frac{t_r^2}{SNR} \tag{2}$$

Where A is the pulse amplitude and $\overline{n^2}$ is the noise variance (N_0B). Given that signal power (S) is $\frac{E}{\tau}$ and noise BW is B, equation (2) can be rewritten as:

$$\overline{{t_0}^2} = \frac{t_r^2 B\tau}{\frac{E}{N_0}} = \frac{1}{\beta^2 \frac{E}{N_0}} \tag{3}$$

Where the last part is due to the relationship between τ, t_r and noise BW (B) resulting in an effective bandwidth dependent on the specific pulse shape. Thermal noise is not the only limiting factor in obtaining the resolution. Direct timing jitter from the transmitter (σ_{TX}), receiver (σ_{RX}) or from phase noise on reference oscillators (σ_{PN}) could also add to the final variance.

$$\overline{{t_0}^2} = \frac{1}{\beta^2 \frac{E}{N_0}} + \sigma_{TX}^2 + \sigma_{RX}^2 + \sigma_{PN}^2 \tag{4}$$

D. Signal-to-Noise Ratio

Another challenge in obtaining effective images through reflections in the microwave, mm-wave regime is the large signal loss in human body. Given that unlike other modalities these losses are the main contrast mechanisms, the system should work with very small SNR levels. Fig.4 shows simulated signal penetration and raw resolution in body fat and fluid based on published models [10]. Penetration depth is plotted for 100dB of tolerated loss and resolution is based on signals with 30% relative BW to carrier. This is a first-order approximation for the "raw" resolution obtainable for each frequency. It is clear that, especially for images involving body fluids, the obtainable resolution becomes smaller than penetration depth for higher frequencies and therefore the low frequency regime has to be simultaneously leveraged.

For the mentioned 100dB loss, frequency BW close to 30-40GHz, and transmit peak power close to 20dBm, the obtained SNR is close to -30 to -40dB. There is a need for large number of array elements as well as long integration windows to improve the SNR levels. Synchronized arrays can generate an increase in transmitted signal power by a maximum of N^2. However, array losses due to lack of perfect synchronization or quantization in delay generation techniques, could result in both power losses as well as pulse widening or "spatial dispersion" (described in section IV-B). Beamforming will also require a wideband delay element to shift the modulated pulse signal in time domain. Narrowband approximations to this delay (fixed phase shifts) will encounter unacceptable errors for larger arrays occupying a wide frequency bandwidth. In this imager, the transmitter uses a delay-locked-loop to move the envelope of the pulse before it is multiplied by the carrier. The carrier phase is also shifted by a narrowband phase shifter. After combining (multiplying) the carrier and the envelope a delayed version of the modulated pulse is obtained and the need for a wideband phase shifter is eliminated.

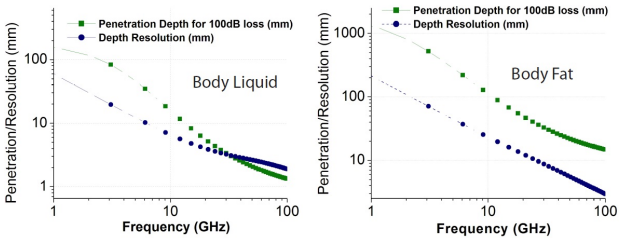

Fig. 4. Penetration depth and resolution (assuming 30% relative BW) for body fat and body liquid.

III. TUSI AS AN ARRAY IMAGER

TUSI implements a time-domain array with a two-tier integration scheme. In the first tier it integrates 2X2 elements on a chip. This is a bi-static setup (separate TX and RX) to reduce direct leakage effects. Time-gating eliminates "delayed" leakage from TX. In the second tier, which enables a scalable array, chips are integrated on daughterboards, multiples of which are then mounted on a common motherboard. The motherboard also integrates clock and power distribution circuits as well as the central processor (Fig.5) . Distributed sampling with partial local computation reduces the aggregate data rate provided to the central processor to a few hundred Mbps.

Several techniques are used to improve the resolution beyond the raw pulse-width limited region. A high pulse repetition frequency (PRF) results in better averaging gain in a given window. TUSI uses frequencies spanning from low microwave to mm-waves to provide flexibility in face of diverse loss mechanisms in different tissue types. In addition, at each of the spectral bands, the center frequency is swept on a batch-by-batch basis to cover the frequency spaces (in the output comb) caused by the high PRF. The center frequency is shifted by multiples of $\frac{PRF}{N}$ (spectral lines are spaced PRF apart). Frequency diversity also allows for removal of ambiguity in range calculations.

The block diagram of the system is shown in Fig.5. This is the block diagram of the high-frequency channel that has both of the antennas integrated on the chip. For lower frequencies the antennas reside on the package/daughterboard. The antennas are designed as a "reticle" and are placed as tiles across the imager.

To reduce the signal dynamic range incident upon the electronic elements, a time-stretched gating circuit is employed. During the averaging period, each "path" will work with a fixed signal level and this reduces the dynamic range.

In the transmitter the timing steps are derived from an interpolating delay-locked loop (shown in Fig.6) [11]. The output of the DLL drives a latch-array that generate controllable short pulses (this performs the time-domain beamforming). This latch-array is designed to reduce the accumulated jitter for longer pulses (by multiple re-timing stages). The same output of the DLL is used to derive the sampler clocks. Using a common clock will reduce the differential jitter between the transmitter and receiver.

To enhance the SNR level at the receiver, extensive signal

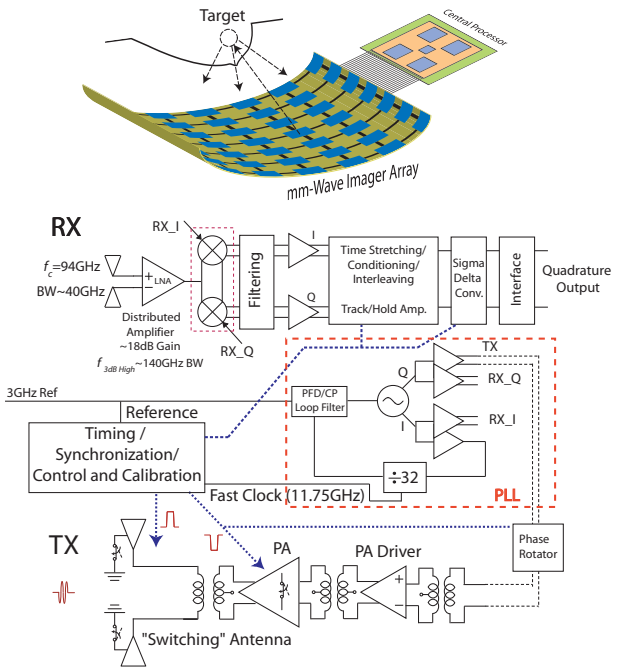

Fig. 5. Proposed array architecture and the block diagram of the TUSI transceiver for the high frequency band.

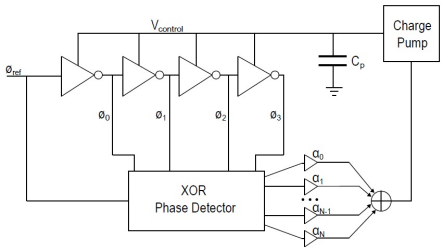

Fig. 6. Delay-Locked Loop architecture for generating fine time steps.

averaging is performed. A sigma-delta modulator is used for data conversion. In the averaging scheme, the quantization noise is shaped through the filter while the white input noise from the receiver sees a "brick-wall" filter (no shaping). For the averaging window of close to 1ms the quantization component of noise will be extensively suppressed. The thermal input noise provides dithering to the sigma-delta converter and this reduces the tones from the limit-cycle oscillations [12].

IV. SOME OF THE CHALLENGES IN LARGE IMAGING ARRAYS

A. Limits of Integration for Closing the SNR Gap

The SNR is improved by $10log(N)$ with having N pulses integrated coherently. The receiver does not use an RF phased-array architecture due to lack of scalability for large apertures. Phase/amplitude errors (from narrow-band approximation as well as from other sources) will limit the resolution in case of RF phase-shifters. Since processing is performed in the digital domain, extensive averaging is performed on the RX to compensate for the low SNR.

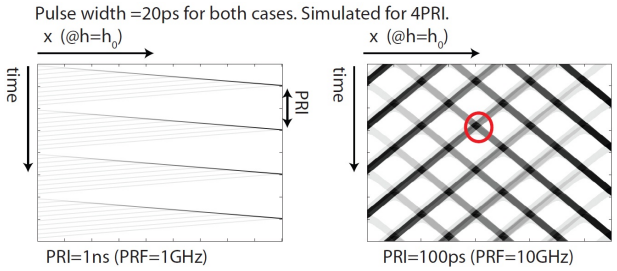

Fig. 7. Received signal (gray-scale coded, dark=large amplitude) at a fixed vertical distance from a 10-element linear sparse-array (at $h = h_0$). The X-axis is the horizontal position (x) and the y axis is time. The array is focused at x=Xmax and simulations are done for 4PRI periods. The circle shows on of the ambiguous points.

However, there are limitations in increasing the averaging window indefinitely.

1) Stability of the imaging setup: Similar to microscopic vibrations that limit optical resolution, macroscopic vibrations lead to spatial filtering of the object and limit the obtainable resolution. Without stabilization techniques, averaging windows are limited to about 10ms-1s, especially for a hand-held imager that is the target of this study.

2) Limitations on increasing pulse repetition frequency (PRF): A repetitive pulse transmission approach is being utilized in which short pulses of width τ are transmitted with a repetition frequency of PRF. Here, given a fixed total integration window, we can increase the number of pulses being averaged by increasing the PRF. However, there are multiple limitations for this approach. First of all, the maximum unambiguous range can limit high PRF as it does in classical radar [8]. In a time-based array system, as proposed here, another limitation rises due to the cross-range ambiguity from high PRF. Intuitively, this is due to the fact that for large arrays and beam angles, the delay spread between first and last element can be quite large. For a far-field array this difference is $(N-1)d\sin(\theta)/v$ where N is the number of elements in array, d is the elements spacing and θ the beam angle from broadside. If the object resides in the near-field of the array, this relationship will be different but in essence one can assume that the delay gets larger with array size. Once this delay difference becomes comparable to the pulse repetition interval (PRI or 1/PRF) secondary "illumination" points will appear and cause ambiguity. Fig.7 shows this effect. This is a gray scale coding of the received amplitude versus horizontal position and time. The arrays are focused to x=Xmax (Fig. 8). In one case (left) the period is chosen to avoid range ambiguity. The second case is for a much higher PRF (same pulse width and distance). Multiple focused points are observed. For illustration purposes a sparse array (large antenna spacing) is chosen to exaggerate secondary focus point amplitudes. In conventional arrays the actual peaks will be smaller.

3) Undesirable coupling of SNR with Resolution through timing errors: In many imaging systems the resolution and SNR are tightly coupled through change of signal energy with pixel size. Improving the resolution often requires better

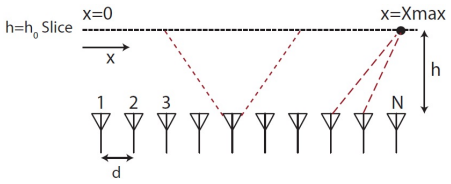

Fig. 8. Linear antenna array with element spacing d. Here, a slice at vertical distance h_0 from the array is being analyzed.

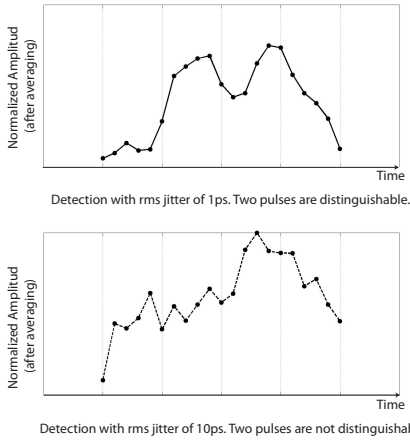

Fig. 9. System simulations of the transmit/receive chain. LO phase noise, transmit and receive jitter, thermal noise and quantization noise effects are included. Two pulses are 25ps wide and are separated by 60ps. The averaging window is assumed to be 1ms with PRF=1GHz. In one case the system has a total rms jitter of 1ps and in the other 10ps.

SNR levels. This is also true for super-resolution techniques that leverage prior knowledge of the waveform. In this imaging modality, jitter limits the number of averaging cycles for a specific target resolution. Sampling and accumulating with a non-ideal clock signal is equivalent to convolving the signal with the probability distribution function (p.d.f.) of the clock arrival edge (in the limit) [13]. For a gaussian p.d.f. of timing jitter with variance of σ^2, the signal is effectively low-pass filtered by a gaussian filter of that bandwidth. Therefore, for long integration times, the image resolution is reduced. This limits the total jitter budget of the transmitter and the receiver to 0.5-5ps depending on range resolution required. Fig.9 shows this effect through transmit/receive system simulations.

B. Accurate Delay Generation

The spatial resolution is a function of the pulse width as well as the delay steps that perform beamforming. The time-step quantization smears multiple reflection points and knocks down or distorts high spatial-frequency components of the image. To calculate the required time-steps, we will first assume a full 180° field-of-view (FOV) for individual antenna elements. With this, we can identify two timing-step requirements. One is related to the relative delay required on two antenna elements when they are focusing on a single point ($\overrightarrow{r} = \overrightarrow{r_0}$). The second is for one antenna element focusing on two adjacent resolution pixels. It could be seen that these problems are geometrically equivalent as long as the array spacing and the pixel sizes are approximately the same dimension. We will analyze the case of adjacent antennas focusing on a single point.

To find the time step we will take the case where we are focusing at a slice with vertical distance h from the array and at $x = 0$ (Fig.8). For $h \gg d$ the worst case will be the delay difference between the first two elements (directly beneath the object). We can approximate this as:

$$\Delta\tau_{min} \simeq \frac{d}{2v} \times \frac{d}{h} = \frac{\frac{d}{2v}}{\alpha} \tag{5}$$

Where d is the antenna spacing. The other extreme case is where $h \ll (N-1)d$ in which the delay difference approaches d/v in the limit. Obviously (5) is the limiting factor in this case. Assuming $PRF = T$ and center frequency of f_0, the maximum range in terms of antenna spacing of half-wavelength (material wavelength or λ_g) is going to be:

$$\alpha = \frac{h_{max}}{d} = \frac{h_{max}}{\lambda/2} = \frac{vT/2}{v/2f_0} = f_0 \times T \tag{6}$$

Here the maximum range is dependent on the PRF. For example for $PRF = 1GHz$ and $f_0 = 90GHz$ we have $\alpha = 90$ and we need a delay step of:

$$\Delta\tau_{min} \simeq \frac{\frac{\lambda/2}{2v}}{\alpha} = \frac{1}{4f_0\alpha} \tag{7}$$

This will translate to $30fs$ timing step which of course is beyond reach. In the calculated scenario, under worst range/cross-range conditions this delay resolution results in no quantization noise. In order to understand the problem we now need to compute the range inaccuracy incurred if there is a quantization noise in delay step. This is yet another way through which resolution (range accuracy) and SNR (ability to energy-combine sources coherently) are coupled. Trading off resolution for SNR is needed especially in cases where deeper signal penetration in tissue is required.

Fig.10 uses a normalized gaussian pulse to illustrate this "spatial distortion". We have assumed a linear incremental quantization error for an array of 100 elements. The quantization error is normalized to the gaussian pulse width. There are four issues arising due to delay quantization: The pulse peak amplitude drops (SNR loss), the peak amplitude moves in position (this needs calibration), the slope reduces (increasing noise effects and increasing the CRLB on ranging accuracy according to (2)) and the pulse width increases (reducing resolution in distinguishing multiple pulses). From Fig.10 it is evident that if the error is within 1% of the pulse width, the error in the final width and slope are within 10% of the ideal case. This result could be generalized to larger or smaller arrays as long as the error bound is scaled accordingly. Our aim is to target a pulse width of 25ps and a delay resolution step close to 1ps (less than 5 %). If better resolution is required, the array will be sub-sampled at the expense of lower SNR.

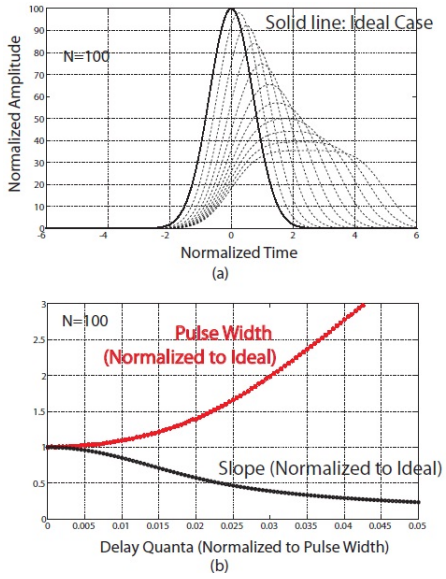

Fig. 10. Effect of minimum delay resolution on array performance. (a) shows the increase in PW as well as change from ideal position. (b) shows the error in PW and slope (compared to ideal) versus minimum delay step (delay quanta). N=100 for simulations.

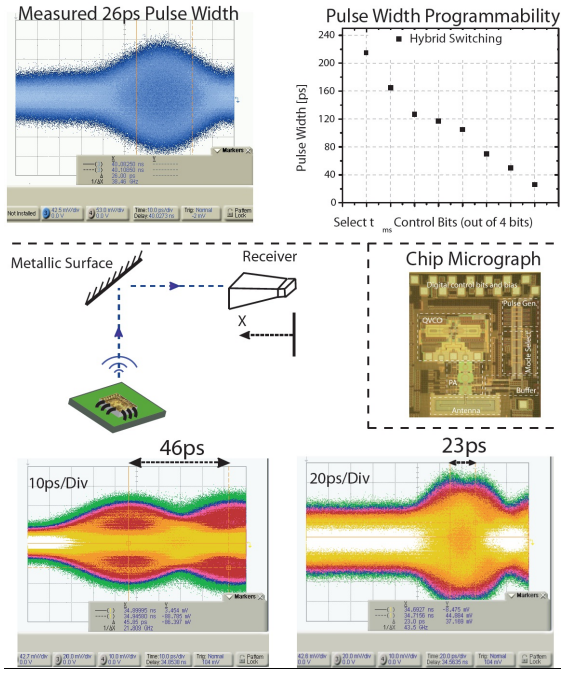

Fig. 11. Measurement summary of the TUSI transmitter prototype. Pulses down to 26ps in width are obtained. Chip micrograph is shown. An experiment to identify range accuracy of the system is also performed in which the position is adjusted and the received data is superimposed.

C. Spatial Coding to Suppress Leakage and Improve Resolution

We propose a spatial coding scheme that can accommodate simultaneous focusing of the beam on multiple locations. Different segments of the two dimensional array concentrate their beams on different parts of the tissue and by that reduce the total scan time that is required for the FOV. To alleviate leakage from adjacent cells, a spatial phase code is enforced on TX/RX on a region by region basis. For example, the phase of the carrier could be adjusted between $0°/180°$ on the TX. The RX in the correct region will also integrate with the right phase coding thereby suppressing the unwanted signals and enforcing the desired reflections. All other adjacent regions will suppress signals intended for this region since their code polarity is different. This technique is complicated by the nature of the object under test (phase of reflections).

D. Other Challenges

There are various other challenges that will not be discussed further. They include amplitude compensation for near-field operation, maintaining a constant group delay in the receiver, maintaining the required antenna beamwidth for FOV, narrow pulse generation, pulse fidelity and echoes, clock jitter and etc.

V. TRANSMITTER PROTOTYPE

A 90GHz-carrier pulsed transmitter was implemented in $0.13\mu m$ SiGe BiCMOS process. To obtain ultra-short pulses with programmable pulse widths, the transmitter employs a number of novel techniques including hybrid switching and Antentronics [2]. The transmit path includes a quadrature VCO, PA driver, PA and the on-chip folded slot antenna with integrated switches. High speed ECL circuits generate and provide the short pulses in several operating modes. The transmitter achieves a record pulse width of 26ps in the hybrid mode and 33ps in the independent mode. This translates to >30GHz of RF BW in the transmitter. The die photo of the chip as well as a summary of the measurements are shown in Fig.11. In this figure, minimum measured pulse width as well as the pulse programmability are illustrated. It also shows an experiment done to assess the resolution capabilities of the transmitter. It is clear that pulses are distinguishable with position adjustment down to 23ps (6.9mm in air). This is with no additional processing.

VI. CONCLUSION

In this paper, some of the challenges of designing a large scale integrated array for medical imaging were discussed. The proposed array combines short transmitted pulses from multiple radiating elements to improve SNR. It also receives the reflections from multiple sites and by that enhances the spatial resolution. In addition to discussing performance limits of the time-based array, challenges related to obtaining higher SNR through averaging, beamforming, spatial dispersion, jitter and timing, and position ambiguity due to large PRF were also addressed. In the end, a transmitter prototype that can support a measured PRF of 1.6GHz and pulse width of 26ps was introduced. This is a first successful step towards a fully integrated portable medical imager.

ACKNOWLEDGEMENTS

The authors acknowledge the contributions of the sponsors of the Berkeley Wireless Research Center, the NSF

Infrastructure Grant No. 0403427, the foundry donation of STMicroelectronics and support under NSF grant ECCS-0702037. Special thanks to Bagher Afshar, Steven Callender, Shinwon Kang and Jun-Chau Chien for valuable discussions and contributions.

REFERENCES

[1] E. C. Fear, et al., "Enhancing breast tumor detection with near-field imaging," Mic. Mag., IEEE, vol.3, no.1 pp.48-56, Mar 2002.
[2] A. Arbabian, *et al.* "A 90GHz Carrier 30GHz Bandwidth Hybrid Switching Transmitter with Integrated Antenna," ISSCC 2010. Dig. of Tech. Papers, pp. 420-421, 3-7 Feb. 2010.
[3] C. Marcu, et al., "A 90nm CMOS Low-Power 60GHz Transceiver with Integrated Baseband Circuitry," ISSCC Dig. Tech. Papers, Feb. 2009.
[4] A. Arbabian and A. Niknejad, "Medical Imaging in Microwave Frequencies," *Poster Presentation*, BWRC Summer Retreat, May 29-31 2007.
[5] A.Arbabian and A. Niknejad, "Time-Domain Ultra-Wideband Synthetic Imager," *Poster Presentation*, BWRC Winter Retreat, Jan. 6-8 2009.
[6] Ries LAG, et al., SEER Cancer Statistics Review, 1975-2000. Bethesda, MD: National Cancer Institute, 2003.
[7] Committee on Technologies for the Early Detection of Breast Cancer, Mammography and Beyond: Developing Technologies for the Early Detection of Breast Cancer, S.J. Nass, et al., Eds. National Cancer Policy Board, NRC 2001.
[8] M. I. Skolnik, Radar Handbook. :McGraw-Hill.
[9] H.L. Van Trees, Detection, Estimation and Modulation Theory, Part 3, John Wiley and Sons, New York, 2001.
[10] C.Gabriel, "Compilation of the dielectric properties of body tissues at RF and microwave frequencies," Report N.AL/OE-TR-1996-0037, Texas (USA), June 1996.
[11] S. Callender, et al., "A Phase-Adjustable Delay-Locked Loop Utilizing Embedded Phase Interpolation," *Proc. RFIC symposium*, Baltimore, June 2011.
[12] J. C. Candy and G. C. Temes, Oversampling Delta-Sigma Data Converters: Theory, Design, and Simulation., 1992. :IEEE Press
[13] T. Miki, H. Yamaguchi and Y. Nagaki, "An accurate wide-band automatic waveform analyzer," *IEEE Trans. Instrum. Meas.*, IM-26, 4 pp. 279-291, Dec. 1977.